HHS Public Access

Author manuscript

Cell Rep. Author manuscript; available in PMC 2023 October 23.

Published in final edited form as:

Cell Rep. 2023 February 28; 42(2): 112109. doi:10.1016/j.celrep.2023.112109.

RTEL1 and MCM10 overcome topological stress during vertebrate replication termination

Lillian V. Campos[1], **Sabrina X. Van Ravenstein**[1], **Emma J. Vontalge**[1], **Briana H. Greer**[2], **Darren R. Heintzman**[1], **Tamar Kavlashvili**[1], **W. Hayes McDonald**[3], **Kristie Lindsey Rose**[3], **Brandt F. Eichman**[2], **James M. Dewar**[1,4,*]

[1]Department of Biochemistry, Vanderbilt University School of Medicine, Nashville, TN 37232, USA

[2]Department of Biological Sciences and Center for Structural Biology, Vanderbilt University, Nashville, TN 37232, USA

[3]Department of Biochemistry and Mass Spectrometry Research Center, Vanderbilt University, Nashville, TN 37232, USA

[4]Lead contact

SUMMARY

Topological stress can cause converging replication forks to stall during termination of vertebrate DNA synthesis. However, replication forks ultimately overcome fork stalling, suggesting that alternative mechanisms of termination exist. Using proteomics in *Xenopus* egg extracts, we show that the helicase RTEL1 and the replisome protein MCM10 are highly enriched on chromatin during fork convergence and are crucially important for fork convergence under conditions of topological stress. RTEL1 and MCM10 cooperate to promote fork convergence and do not impact topoisomerase activity but do promote fork progression through a replication barrier. Thus, RTEL1 and MCM10 play a general role in promoting progression of stalled forks, including when forks stall during termination. Our data reveal an alternate mechanism of termination involving RTEL1 and MCM10 that can be used to complete DNA synthesis under conditions of topological stress.

In brief

*Correspondence: james.dewar@vanderbilt.edu.

AUTHOR CONTRIBUTIONS

D.R.H. performed the experiments outlined in Figures 1 and S1. K.L.R. performed the mass spectrometry, and W.H.M. analyzed the results. *Xenopus* Mcm10 was purified by B.H.G. T.K purified LacR and performed 2D gel experiments. S.X.V. performed experiments shown in Figures 3D, S2G, S4D–S4G, and S6D–G. S.X.V and L.V.C performed plasmid pull-down experiments. E.J.V. generated a new antibody targeting RTEL1 and performed the experiments shown in Figures S2H–S2J. L.V.C. carried out all other experiments. J.M.D. designed and supervised the project. The manuscript was written by J.M.D. and L.V.C. with input from B.F.E., K.L.R., and W.H.M.

DECLARATION OF INTERESTS

The authors declare no competing interests.

SUPPLEMENTAL INFORMATION

Further information can be found online at https://doi.org/10.1016/j.celrep.2023.112109.

INCLUSION AND DIVERSITY

One or more of the authors of this paper self-identifies as an underrepresented ethnic minority in their field of research or within their geographical location.One or more of the authors of this paper received support from a program designed to increase minority representation in their field of research.

Topological stress can stall DNA replication forks during the stage of replication termination. Campos et al. find that the helicase RTEL1 and the replication protein MCM10 allow replication forks to overcome stalling during termination. They show that RTEL1 and MCM10 form an alternative mechanism of termination operating under topological stress.

Graphical Abstract

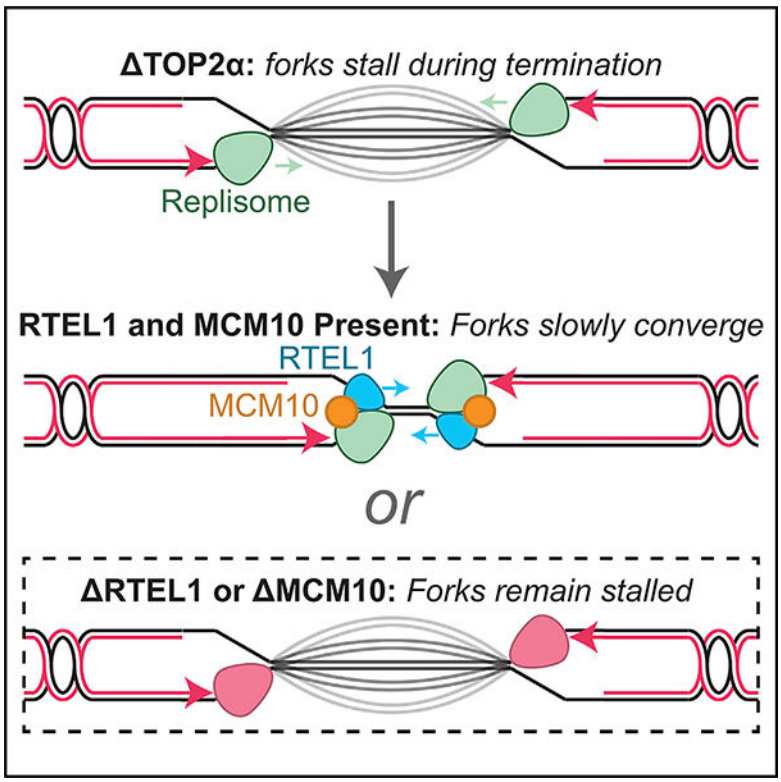

INTRODUCTION

Eukaryotic DNA replication is organized into discrete steps: initiation, elongation, and termination.[1–4] This scheme occurs ~60,000 times per S phase in human cells[5] and must be executed faithfully to ensure genome stability. An excess of pre-replication complexes (pre-RCs) are loaded onto DNA but only a subset of these are activated.[6] This allows for defects in initiation or elongation to be overcome by activation of a proximal pre-RC, resulting in a new initiation event.[7] Additionally, elongation defects can be overcome by a wide array of DNA damage responses that can aid fork progression.[8] In contrast to initiation and elongation, much less is known about how obstacles to termination of DNA synthesis are overcome. This is important to address because it is well established that terminating replication forks are susceptible to stalling during SV40 replication,[9,10] and recent data suggest the same is also true in eukaryotes.[11,12]

Resolution of topological stress is particularly important during termination of DNA replication (Figure S1A) compared with earlier stages of replication. Type II topoisomerases are important to prevent converging replication forks from stalling during viral,

bacterial, yeast, and vertebrate replication termination.[11,13–15] The unique role of type II topoisomerases is thought to reflect their ability to resolve intertwines of double-stranded DNA that form behind replication forks, ("pre-catenanes"), which cannot be removed by other topoisomerases.[16–18] Without TOP2 activity, pre-catenanes accumulate either during termination[19,20] or throughout replication[15] and cause replication forks to stall due to topological stress (Figure S1B). However, replication forks can ultimately complete DNA synthesis without type II topoisomerases (Figure S1B).[11,13–15,21] These data suggest that additional mechanisms exist that can overcome topological stress as replication forks converge.

Two mechanisms have been identified that promote resolution of converging forks independent of type II topoisomerases. In budding yeast, the 5′−3′ helicases Rrm3 and Pif1 both promote fork merger during replication termination.[11] These proteins, as well as their fission yeast paralog Pfh1, are also implicated in replication through, and termination at, replication barriers,[22–24] suggesting that the obstacles posed by termination and replication barriers may be resolved by similar mechanisms. In bacteria, the RecQ helicase can cooperate with topoisomerase III to resolve converging forks independent of type II topoisomerase activity.[25] However, budding yeast topoisomerase III (Top3) is unable to promote resolution of converging forks.[11] Thus, type II topoisomerases and 5′−3′ helicases are the only proteins implicated in fork convergence in eukaryotes. However, it is unclear whether this is true in vertebrates and whether other proteins might promote fork convergence.

To identify proteins that might promote fork merger independently of type II topoisomerases, we performed a mass spectrometry analysis of proteins bound to DNA in TOP2α-immunodepleted *Xenopus* egg extracts. We found that the 5′−3′ helicase RTEL1 and the replisome component MCM10 were highly enriched on DNA under these conditions. We show that RTEL1 and MCM10 are crucially important when forks stall during termination due to the absence of TOP2α. RTEL1 and MCM10 function is non-additive, both proteins co-immunoprecipitate, and MCM10 promotes RTEL1 recruitment to DNA. These observations suggest that MCM10 and RTEL1 form a single functional unit. RTEL1 and MCM10 do not affect utilization of TOP2α during DNA replication, indicating that they do not regulate pre-catenane generation but are both important for fork progression through a replication barrier, independent of any effects on termination. Our data show that RTEL1 and MCM10 facilitate fork progression through multiple obstacles to DNA replication and promote an alternate pathway for replication termination that allows replication forks to overcome topological stress.

RESULTS

A proteomic screen for proteins bound to terminating replication forks

To identify proteins that might promote fork merger independently of type II topoisomerases, we performed a proteomic analysis of proteins bound to replicating DNA when TOP2α, which is the TOP2 isoform involved in DNA replication,[15] was removed or inhibited. Under these conditions, replication forks stall during termination due to accumulation of topological stress.[15] Plasmid DNA was replicated in mock-immunodepleted

(mock-depleted) or TOP2α-immunodepleted (TOP2α-depleted) *Xenopus* egg extracts as previously described.[15] In parallel, replication was performed in the presence of the TOP2 inhibitor ICRF-193 ("TOP2-i") as an alternate means of preventing TOP2 activity.[15] Chromatinized plasmid DNA was recovered 18 min after the onset of DNA synthesis, when most forks have normally merged but are stalled when TOP2 activity is prevented (Figure 1A).[15] Chromatin-bound proteins were then analyzed by chromatin mass spectrometry and quantified by label-free quantification, as previously described.[26–28] This approach identified a total of 495 proteins (Table S1). Importantly, TOP2α was ~200-fold reduced in TOP2α-depleted conditions compared with the mock (Figure S1C), consistent with effective removal of TOP2α from the extracts. Additionally, TOP2α was ~60% enriched in the presence of TOP2-i compared with the mock (Figure S1C), consistent with the ability of TOP2-i to trap TOP2 on DNA.[29] Thus, this dataset contains proteins that are chromatin-bound during normal DNA replication and when TOP2 is either absent or inhibited.

We next searched our dataset for proteins that exhibited increased DNA binding when TOP2 was either absent or inhibited. We selected proteins that were ≥2-fold enriched in TOP2α-depleted and TOP2-i-treated conditions compared with the mock condition (Figure S1C, Table S2). We identified 40 proteins, and in all cases, enrichment was statistically significant ($p \leq 0.05$) for at least one of the two comparisons (Figures 1B and S1C). We then categorized the proteins based on their previously reported functions. Most proteins (36) function at and/or travel with replication forks (Figures 1B and S1C). This is consistent with fork stalling during termination, which prevents removal of replication proteins from DNA.[15] We identified three proteins that are implicated in DNA damage responses (Figures 1B and S1C), which may reflect responses to replication fork stalling. We also identified filamin-A (FLNA), which could not readily be categorized. FLNA promotes branching of actin filaments, which play a role during DNA replication in this extract system.[30] Additionally, FLNA has been implicated in the DNA damage response.[31] Thus, enrichment of FLNA could reflect a role in either DNA replication or DNA damage. Importantly, most replication fork and DNA damage proteins were ~2- to 8-fold enriched in both conditions (Figure 1B). However, five proteins were appreciably further enriched in both conditions. The PCNA loader RFC1 and the lagging strand DNA polymerase δ subunits DPOD1 and DPOD2 were ~8- to 16-fold enriched. Enrichment of these proteins could reflect the switch from DNA synthesis by leading strand polymerase ε to polymerase δ, which was suggested to occur during replication termination.[32] The two remaining proteins, RTEL1 and MCM10, were ~32- to 64-fold enriched. Thus, based on enrichment alone, RTEL1 and MCM10 were the strongest candidates revealed by our analysis.

RTEL1 is a $5'-3'$ DNA helicase that can unwind DNA ahead of a stalled replication fork to help overcome obstacles to fork progression.[33] Additionally, analogous $5'-3'$ helicases from yeast have been implicated in resolution of termination replication forks in cells and reconstituted systems, suggesting that the same may be true for RTEL1.[11,22–24] MCM10 promotes replicative helicase activity[34] and is important for replication initiation.[35] MCM10 is also implicated in replisome stability, which could be important to overcome fork stalling during termination.[36,37] Thus, based on the reported activities of RTEL1 and MCM10, these proteins are ideally suited to promote resolution of terminating replication forks.

RTEL1 and MCM10 promote replication fork merger

We next tested whether RTEL1 promotes replication termination. To this end, we replicated plasmid DNA in mock-immunodepleted ("mock-depleted") extracts or RTEL1-immunodepleted ("RTEL1-depleted") extracts; then we monitored the formation of the final products of replication as a readout for termination (Figure 2A). In mock-depleted extracts, the final products were circular monomers (Figure 2Aiii, CMs, Figure 2B, lanes 2–6) as expected.[38] In RTEL1-depleted extracts, formation of circular monomers was delayed (Figure 2B, lanes 1–6 and 13–18), and there was no appreciable impact on total DNA synthesis (Figure S2A). Thus, the delay in circular monomer formation was due to a termination defect, rather than a defect during initiation or elongation of DNA synthesis. Importantly, θ structures (Figure 2Ai, θs) persisted in RTEL1-depleted extracts (Figure 2B, lanes 1–6 and 13–18), demonstrating that the delay in circular monomer formation was due to a fork merger defect. The minimally catenated catenanes (Figure 2Aii) that normally form during termination[38] were not detected in these experiments, presumably due to the lack of synchrony. We therefore quantified circular monomers (Figure 2Aiii), which arise from these minimally catenated catenanes (Figure 2Aii), as a readout for fork merger (Figures 2Ai–ii). Quantification of circular monomers confirmed a modest delay in fork merger in RTEL1-depleted extracts (Figure 2C). Thus, fork merger was delayed upon RTEL1 depletion, consistent with the involvement of analogous 5′−3′ helicases in fork merger in other eukaryotic systems.[11,22–24]

RTEL1 was enriched on DNA when replication forks were stalled due to loss of TOP2 activity (Figure 1B). To test whether RTEL1 was particularly important for fork merger under these conditions, we monitored the final products of replication in TOP2α-depleted and TOP2α-RTEL1-depleted (i.e., double depleted of both TOP2α and RTEL1) extracts. In TOP2α-depleted extracts, the final products of replication (Figure 2B, lanes 9–12) were highly catenated catenanes (Figure 2A, Cats+), which arise from fork merger and are slowly converted to less-catenated species (Figure 2B, Cats−) by residual TOP2 activity.[15] In TOP2α-RTEL1-depleted extracts, formation of catenanes (Cats+ and Cats−) was dramatically impaired (Figure 2B, lanes 7–12 and 19–24). Catenanes formed in TOP2α-RTEL1-depleted extracts were predominantly Cats− (Figure 2B, lanes 23–24), presumably because the prolonged fork stalling allowed for more unlinking by residual TOP2 prior to fork merger. Additionally, θ structures persisted at late time points in TOP2α-RTEL1-depleted extracts compared with TOP2α-depleted extracts (Figure 2B, lanes 7–12 and 19–24). Catenane formation was quantified as a readout for fork merger (Figure 2C), which showed that the difference in fork merger between TOP2α-depleted and TOP2α-RTEL1-depleted extracts was much greater than between mock-depleted and RTEL1-depleted extracts. 2D gel analysis of replication fork structures confirmed that this difference reflected a fork merger defect, rather than any other alteration in replication fork structure (Figures S2D and S2E). The RTEL1 antibody was previously verified to be specific to RTEL1.[33] Additionally, a second RTEL1 antibody raised in this study reproduced the same effect (Figures S2F and S2J), further demonstrating that the effects observed in this study were specific to RTEL1. However, we were unable to rescue the RTEL1 depletion effect with purified RTEL1 protein, so it is possible that RTEL1 fulfills this role as part of a

larger complex. Overall, these data show that RTEL1 becomes crucial for fork merger when TOP2α activity is lost.

To address whether MCM10 also promotes fork merger, we performed the same analysis as with RTEL1 (above). In MCM10-depleted extracts, formation of circular monomers was modestly delayed (Figure 2D, lanes 1–6 and 13–18), but this could be attributed to slowed replication (Figure S3A). Importantly, this delay had little impact on the fraction of circular monomers produced (Figure 2E), indicating that there was negligible effect on termination. Instead, the delay in formation of circular monomers was likely due to delayed initiation of DNA replication, as previously described.[36,39] In TOP2α-MCM10-depleted extracts, formation of catenanes was dramatically impaired (Figure 2D, lanes 7–12 and 19–24, Figure 2E), and θ structures persisted at late time points (Figure 2D, lanes 7–12 and 19–24), suggesting a fork merger defect. In support of this conclusion, 2D gel analysis revealed the persistence of converging forks and other structures arising from termination defects (Figures S3D and S3E). However, a slight increase in DNA structures arising from earlier stages of DNA replication was observed (Figures S3D and S3E), consistent with the overall replication defect in MCM10-depleted extracts (Figures S3A and S3C). Importantly, when the delay in replication in MCM10-depleted extracts was accounted for, a clear delay in fork merger was observed (Figure S3F), demonstrating that fork merger was delayed in TOP2α-MCM10-depleted extracts compared with TOP2α-depleted extracts. The fork merger defect observed in TOP2α-MCM10-depleted extracts was rescued by re-addition of recombinant *Xenopus* MCM10 (Figures S3G and S3H), which confirmed that the fork merger defect was due to loss of MCM10 alone. These data show that MCM10 normally plays a negligible role in promoting replication fork merger but becomes important when TOP2α activity is lost. Overall, our results show that RTEL1 and MCM10 are crucial to overcome topological stress during replication termination.

RTEL1 and MCM10 cooperate during fork merger

RTEL1 and MCM10 exhibited similar levels of binding in our proteomic analysis (Figure 1) and were both crucial for fork merger following inactivation of Top2α (Figure 2). To address whether RTEL1 and MCM10 function together, we tested whether depletion of both proteins together resulted in a non-additive effect compared with depletion of either protein alone. This could not be done in TOP2α-depleted extracts because depletion of three proteins would compromise extract function. Instead, we depleted either one or both proteins in the presence of a low dose of TOP2-i, which also inhibits fork merger.[15] Low-dose TOP2-i led to formation of several catenated species that migrated similarly to θ structures (Figure S4A, lanes 1–6), which made it challenging to measure products of fork merger. We therefore purified DNA intermediates and performed restriction digests to eliminate topoisomers (Figure 3A). This allowed us to directly monitor fork merger by measuring conversion of double Y structures to the linear products of fork merger (Figure 3A). Under these conditions, fork merger was largely complete by 60 min (Figure 3B, lanes 1–6, and Figure 3C). RTEL1 depletion delayed fork merger by ~80 min (Figure 3B, lanes 7–12, and Figure 3C), while MCM10 depletion delayed fork merger by ~20 min (Figure 3B, lanes 13–18, and Figure 3C), consistent with a fork merger being more dependent on RTEL1 than MCM10 (Figure 2). However, fork merger was not further delayed following RTEL1-

MCM10 depletion compared with RTEL1 depletion alone (Figure 3B, lanes 7–12 and 19–24, and Figure 3C). Similar results were obtained when loss of θ structures was measured as a readout for fork merger (Figure S4B). There was little impact on total DNA synthesis in all conditions tested (Figure S4C), indicating that these differences were due to defects in termination rather than earlier stages of DNA synthesis. The same experiment was then repeated in the absence of TOP2-i (Figures S4E–S4G). MCM10 depletion modestly slowed replication in RTEL1-depleted extracts (Figures S4F) but did not appreciably exacerbate the fork merger defect induced by RTEL1 depletion (Figure S4G), consistent with the results obtained in the presence of TOP2-i (Figures 3A–3C). Overall, these data show that MCM10 and RTEL1 function together to promote fork merger in the presence of topological stress.

Since MCM10 and RTEL1 function together, we wondered whether they might also physically interact. To address this, we performed co-immunoprecipitation (coIP) experiments and analyzed the immunoprecipitates by western blotting. Immunoprecipitation of RTEL1 led to coIP of MCM10 (Figure 3D, lanes 5 and 6) and vice versa (Figure 3D, lanes 5 and 7), consistent with previous identification of MCM10 as an interacting partner of RTEL1 in murine cells.[40] RTEL1 was also previously reported to interact with the DNA sliding clamp PCNA,[40] but coIP was not detected between RTEL1 and PCNA in *Xenopus* egg extracts (Figure 3D, lanes 5 and 6), suggesting that the interaction is either too weak to detect under these conditions or not conserved in *Xenopus* egg extracts. Importantly, coIP was also not detected between MCM10 or RTEL1 and replicative helicase components (Figure 3D, MCM6, MCM7, CDC45), the origin recognition complex (Figure S5A, ORC2), or the single-stranded DNA binding protein RPA (Figure S5A, RPA30). Thus, the interaction between MCM10 and RTEL1 did not reflect binding of either protein to a wide array of replication proteins. *Xenopus* egg extracts are DNA free and were not supplemented with DNA for these experiments, indicating that the interaction was not DNA dependent. Accordingly, the interaction was still detected when we used an alternative coIP protocol that involved pre-treatment with Benzonase nuclease (Figure S5B). Thus, the interaction between RTEL1 and MCM10 is specific and not bridged by DNA. Immunoprecipitation of TOP2α led to weak coIP with RTEL1 (Figure 3D, lanes 5 and 8), but the reciprocal interaction was not detected (Figure S5A, lanes 5 and 6), indicating that there was no significant interaction between RTEL1 and TOP2α. Additionally, immunoprecipitation of TOP2α did not result in coIP with MCM10 (Figure 3D, lanes 5 and 8) and vice versa (Figure S5A, lanes 5 and 7). These data show that RTEL1 and MCM10 physically interact, either directly or indirectly, and this does not reflect binding of either RTEL1 or MCM10 to a wide array of replication proteins or to DNA.

To investigate the significance of the RTEL1-MCM10 interaction, we next tested whether either RTEL1 or MCM10 influence the other's recruitment to replication forks. Plasmid DNA was replicated in RTEL1- or MCM10-depleted extracts in the presence of TOP2-i to stall forks during termination (as in Figure 1 and Heintzman et al.[15]). Chromatin-bound proteins were then recovered so that the abundance of RTEL1 and MCM10 could be analyzed. RTEL1 depletion reduced MCM10 binding at early time points (Figure S5D, 10 min), which could reflect their cooperation during earlier stages of DNA replication (Figures S4E–S4G). However, at later time points, when the role of RTEL1 during termination was most significant (Figure 3C, 30 min), RTEL1 did not affect MCM10 binding (Figure S5E,

30 min). Thus, although RTEL1 did contribute to MCM10 binding, this was unlikely to be relevant to termination. In contrast, MCM10 depletion reduced RTEL1 binding at all time points analyzed (Figures S5G–S5I, 10 min and 30 min). CDC45 and PCNA levels were reduced in MCM10-depleted extracts at early time points (Figure S5H, 10 min) but not at later time points (Figure S5I, 30 min) when the termination defect was most apparent (Figure 3C, 30 min). At this point an ~50% reduction in RTEL1 binding was observed (Figure S5J). Thus, MCM10 makes a substantial contribution to RTEL1 binding but is not absolutely required. Importantly, RTEL1 depletion had no detectable impact on DNA synthesis, and MCM10 depletion resulted in only a slight delay (Figure S4C), so these effects are unlikely to be due to slowed replication. Our observations suggest that MCM10 may promote RTEL1 binding during termination, but additional work will be required to formally test whether this is the case.

MCM10 and RTEL1 do not limit the need for TOP2 activity

Depletion of TOP2α causes replication forks to stall due to accumulation of catenanes.[15] Thus, the role of RTEL1 and MCM10 in promoting fork merger could be explained by negative regulation of catenane formation, which would limit the need for TOP2α activity. We were unable to unambiguously measure catenanes, as this can only performed using fully replicated molecules generated in the absence of TOP2,[15] and co-depletion of either MCM10 or RTEL1 would interfere with formation of these same fully replicated molecules (Figure 2). As an alternative strategy, we tested whether RTEL1 or MCM10 affects the abundance of TOP2:cleavage complexes (TOP2:CCs) generated by the TOP2 poison etoposide. TOP2:CCs arise when the TOP2 catalytic cycle is blocked and thus should act as a readout for TOP2 activity.[41] If RTEL1 or MCM10 normally negatively regulate catenane formation, then loss of either protein would be expected to increase the abundance of TOP2:CCs.

We have previously shown that etoposide causes formation of TOP2:CCs during replication in *Xenopus* egg extracts.[42] To carefully quantify the formation of TOP2:CCs, we first replicated plasmid DNA in the presence of a low dose of etoposide (Figure 4A). Reactions were stopped at different time points and mixed with a small amount of fully replicated control plasmid (pCTRL) that served as a loading control (Figure 4A). Each reaction was then split in half and either left untreated or treated with proteinase K to remove TOP2:CCs (Figure 4A). DNA was then subjected to phenol:chloroform extraction, which purified only DNA molecules that did not contain TOP2:CCs (Figure 4A). This assay acts as a highly sensitive readout for TOP2:CC formation because even a single DNA-protein crosslink (DPC) is sufficient to retain the DNA in the organic phase and prevent its recovery in the aqueous phase.[43] DNA molecules purified from the aqueous phase were separated on native agarose gels to detect molecules that did not contain TOP2:CCs (Figure 4B, −ProtK, “No DPCs”) or total DNA molecules (Figure S6A, +ProtK, “Total”). This allowed us to calculate the percentage of molecules that contained TOP2:CCs (Figure 4C). Etoposide treatment caused θ structures and nicked molecules to persist (Figures S6A, lanes 1–4, 9–12). However, these molecules were lost when proteinase K treatment was omitted (Figure 4B, lanes 1–4, 9–12), indicating that they contained TOP2:CCs. When we calculated the percentage of DPC-containing molecules, we found that ~75% of molecules

contained DPCs, and this declined by ~2-fold over the course of our experiments (Figure 4C). Importantly, most DPCs formed under these conditions were replication dependent (Figures S6D–S6G). Thus, our experimental approach allowed us to monitor formation of a sub-saturating quantity of TOP2:CCs during DNA replication that were gradually resolved.

To test whether RTEL1 or MCM10 affected the abundance of TOP2:CCs, we monitored the abundance of DPCs in extracts that were either RTEL1 depleted (Figures 4B, 4C, and S6A–S6C) or MCM10 depleted (Figures 4D, 4E, and S6H–S6J). When proteinase K was omitted, the abundance of DPC-free DNA molecules was not appreciably reduced by either RTEL1 depletion (Figure 4B, lanes 9–16) or MCM10 depletion (Figure 4D, lanes 9–16), indicating that neither depletion appreciably increased abundance of TOP2:CCs. Quantification of DPC-containing molecules also revealed little difference between mock and depleted conditions following etoposide treatment (Figures 4C and 4E). Although resolution of DPCs was delayed by ~10 min following MCM10 depletion (Figure 4E), this was likely due to the ~10 min delay in total DNA replication under these conditions (Figure S6I). Overall, these data show that RTEL1 and MCM10 do not appreciably impact formation of DPCs following etoposide treatment and thus do not negatively regulate catenane generation.

RTEL1 and MCM10 promote fork progression through a replication barrier

The requirement for RTEL1 and MCM10 following inactivation of TOP2α (Figure 2) could reflect a general role for RTEL1 and MCM10 in responding to fork stalling. Accordingly, RTEL1 is important for fork progression when two forks converge upon a LacR-bound *lacO* array, which functions as a replication barrier.[33] However, it is unclear whether this reflects a general role in fork progression or a specific role during termination. Thus, we investigated the roles of RTEL1 and MCM10 in fork progression through a replication barrier, using a strategy that could determine whether any observed differences were due to fork progression or termination. We monitored the ability of replication forks to complete DNA synthesis within LacR arrays, which act as barriers to fork progression.[38] We compared fork merger in LacR-bound plasmids containing 16x (p[*lacO*x16]) or 32x (p[*lacO*x32]) copies of *lacO* (Figure 5A). In both cases only a single termination event takes place. However, replication forks must overcome approximately twice as many bound LacR molecules in p[*lacO*x32] compared with p [*lacO*x16]. Thus, if RTEL1 or MCM10 depletion confers a termination defect, then the delay compared with the mock condition should be similar for p[*lacO*x16] and p[*lacO*x32]. However, if a general fork progression defect is observed, then the delay should be approximately twice as great in the depletion condition compared with the mock.

We first tested the role of RTEL1 in promoting fork progression through a LacR array. Replication of p[*lacO*x16] and p[*lacO*x32] led to formation of several catenated species (Figure S7A), so restriction digests were performed on purified DNA to allow unambiguous quantification of fork merger (Figure 5A, as in Figure 3A). Double-Ys persisted and formation of linear products was delayed during replication of both p[*lacO*x16] (Figure 5B, lanes 5–8, Figure 5C) and p[*lacO*x32] (Figure 5D, lanes 5–8, Figure 5E) in RTEL1-depleted extracts, as expected.[33] Importantly RTEL1 depletion caused an ~30 min delay in fork merger during replication of p[*lacO*x16] and an ~60 min delay during replication

of p[*lacO*x32] (Figure S7D). Because the extent of the delay is approximately doubled when the size of the LacR array is doubled, this shows that RTEL1 plays a general role in promoting fork progression through a replication barrier that is not confined to termination.

We next tested the role of MCM10, as described for RTEL1 (above). Fork merger was also delayed during replication of both p[*lacO*x16] (Figure 5F, lanes 5–8, Figure 5G) and p[*lacO*x32] (Figure 5H, lanes 8–12, Figure 5I) in MCM10-depleted extracts. MCM10 depletion caused an ~10 min delay in fork merger during replication of p[*lacO*x16] and an ~40 min delay during replication of p[*lacO*x32] (Figure S7G). Thus, MCM10 also plays a general role in promoting fork progression through a replication barrier that is not confined to termination. Because MCM10 depletion delayed fork merger ~4-fold during replication of p[*lacO*x32] compared with p[*lacO*x16], this also suggested that MCM10 became more important as the duration of the stall increased. Importantly, none of these effects could be attributed to slowed replication in MCM10-depleted extracts because the ~10 min delay in replication (Figures S3A and S3C) had negligible impact on these experiments, where reactions were sampled every 20 min (Figures S7H–S7J). Overall, these data show that MCM10 plays a general role in promoting fork progression through a replication barrier that is not confined to termination. Thus, both RTEL1 and MCM10 promote fork progression through replication barriers, independent of any role during termination.

DISCUSSION

Multiple mechanisms for replication termination

Our data support a multi-faceted model for vertebrate replication termination (Figure 6). Ordinarily, efficient resolution of catenanes by TOP2 ensures rapid fork merger (Figure 6Ci). If TOP2 is unable to fulfill this role, then replication forks stall (Figure 6Cii), and fork merger occurs slowly, promoted by RTEL1 and MCM10, which cooperate to ensure continued progression of stalled forks. Thus, our data show that vertebrate termination involves multiple mechanisms and implicates a core replisome protein, MCM10, in this process.

RTEL1 and MCM10 promote fork merger in the absence of TOP2 activity. Under these conditions the final products of replication are catenanes (Figure 6Dii), which would need to be resolved to allow chromosome separation during mitosis. TOP2-independent mechanisms of unlinking catenanes have not been described, and these species would be expected to undergo chromosome breakage upon exit from mitosis[44] unless TOP2-independent mechanisms of catenane unlinking exist.

Similarities and differences between vertebrate and yeast termination

Maximal replication fork merger in the budding yeast reconstituted system requires both 5′−3′ helicase activity and topoisomerase activity, provided by both Top1 and Top2.[11] The 5′−3′ helicase Rrm3 is normally crucial for termination, while Top2 makes a minor contribution to fork merger,[11] consistent with cellular data.[21] Although another study reported a more significant role for Top2 during fork convergence in yeast cells,[45] this was only for a minority of termination events,[46] consistent with a minor role for Top2. In

contrast, loss of TOP2α or RTEL1 results in a pronounced defect in vertebrate termination (Figure 2 and Heintzman et al.[15]). Another difference is that yeast topoisomerases and 5′−3′ helicases appear to act in an additive fashion, suggesting that they function independently. In contrast, elimination of either TOP2α *or* RTEL1/MCM10 function results in a much lesser termination defect than elimination of both TOP2α *and* RTEL1/MCM10. This suggests that TOP2α and RTEL1/MCM10 share overlapping function. Thus, although similar mechanisms (topoisomerases and 5′−3′ helicases) promote fork merger in both the yeast and vertebrate systems, the priority placed on these mechanisms differs, and the relationship between these mechanisms appears to differ.

The role of RTEL1

RTEL1 is crucial for termination when TOP2 activity is compromised (Figures 2B and 2C, ΔTOP2α vs. ΔTOP2α ΔRTEL1, Figures 6Cii–Dii), but it is also important for fork merger under otherwise unperturbed conditions (Figures 2B and 2C, Mock vs. ΔRTEL1, Figures 6Ci–6Di) when fork stalling does not ordinarily occur.[38] In both cases, the most likely function of RTEL1 is to unwind DNA ahead of forks, as previously described.[33] Interestingly, MCM10 supports RTEL1 in response to topological stress (Figures 3A–3C) but makes minimal contribution under unperturbed conditions (Figures 2D and 2E, Mock vs. ΔMCM10). This may suggest that RTEL1 fulfills different roles during unperturbed termination (Figures 6Ci–6Di) and in response to topological stress (Figures 6Cii–6Dii).

The role of MCM10

The role we have identified for MCM10 in promoting replication fork convergence cannot be explained by existing models for MCM10 function. Yeast MCM10 is important for activation of the replicative helicase and initiation of DNA synthesis.[35] However, we observe initiation is only slightly delayed (Figures 2D, S3A, and S3C). These observations are consistent with previous reports that MCM10 is important for initiation but not required.[36] However, it is possible that in both cases MCM10 depletion is incomplete, and low levels of residual MCM10 are sufficient for initiation. Either way, initiation defects cannot account for the fork merger defect we observe (Figure S3F). Yeast MCM10 promotes bypass of lagging strand obstacles by facilitating isomerization of the CMG helicase.[34] Importantly, CMG isomerization does not promote bypass of leading strand obstacles, and the obstacles we assess here (topological stress in Figure 2 and DNA-bound proteins in Figure 5) affect both strands equally. It is thus unlikely that MCM10 promotes fork merger by facilitating CMG isomerization. Finally, both yeast and vertebrate MCM10 were reported to promote replisome stability.[36,37] However, we observe similar levels of the replication proteins CDC45 and PCNA on DNA at late time points (Figure S5I). Thus, the function of MCM10 that we have identified cannot be explained by previously described functions.

RTEL1 and MCM10 functionally cooperate (Figures 3A–3C). Additionally, MCM10 promotes, but is not required for, RTEL1 binding (Figures S5G–S5J), while RTEL1 does not impact MCM10 binding during termination (Figures S5C–S5F). Thus, our favored model is that MCM10 promotes RTEL1 recruitment. This would explain why loss of RTEL1 results in a much more dramatic fork merger defect than loss of MCM10 alone (Figure 3C). Given that RTEL1 and MCM10 physically interact (Figure 3D), our favored model is

that MCM10 promotes recruitment of RTEL1 to replication forks by directly binding to it. However, further studies will be required to test whether this is the case. Because RTEL1 and MCM10 also promote fork progression during telomere replication,[47,48] the mechanism of cooperation might apply to processes other than termination.

Relevance to *in vivo* settings

Our experiments were performed using circular chromatinized plasmids that lack chromosomal features (e.g., centromeres) and many aspects of chromosome metabolism (e.g., transcription). It will therefore be important to test our model within the context of full-length chromosomes in cells. However, we note that the basic mechanism of fork merger and the roles of $5'-3'$ helicases in fork merger were elucidated from *in vitro* systems[11,38] and also were shown to operate *in vivo*,[11,49] so it would be surprising if the mechanism we have described did not apply in cells.

Limitations of the study

We were unable to rescue the RTEL1 depletion effect with purified recombinant protein, so it is possible that the role we have described for RTEL1 is carried out by a larger protein complex. Although we report a physical interaction between RTEL1 and MCM10, we did not reconstitute this interaction using purified proteins, so we cannot say whether the interaction is direct. Additionally, RTEL1 and MCM10 likely have roles during earlier stages of DNA replication, which are not addressed by this study. Finally, it is also possible that there may be differences between termination in the *Xenopus* egg extracts used in this study and within a cellular environment.

STAR★METHODS

RESOURCE AVAILABILITY

Lead contact—Further information and requests for resources and reagents should be directed to and will be fulfilled by the Lead Contact, James Dewar (james.dewar@vanderbilt.edu).

Materials availability—Antibodies, proteins, and plasmids generated in this study are available without restriction upon request. No other unique reagents were generated.

Data and code availability

- Proteomic data have been deposited at ProteomeXchange and are publicly available as of the date of publication. The accession number is listed in the key resources table.
- This paper does not report original code.
- Any additional information required to reanalyze the data reported in this paper is available from the lead contact upon request.

EXPERIMENTAL MODEL AND SUBJECT DETAILS

Xenopus laevis—Egg extracts were prepared using sexually mature female *Xenopus laevis* (Nasco #LM0053MX, LM00715MX). All experiments involving animals were approved by the Vanderbilt University International Animal Care and Use Committee.

METHOD DETAILS

Xenopus* egg extracts—Xenopus* egg extracts were prepared from *Xenopus laevis* wild type males and females (Nasco) as previously described[58] and summarized briefly below.

To prepare Crude Interphase Extract (CIE), 6–18 female frogs were each injected with 80 IU of human chorionic gonadotrophin (HCG). 2–7 days later, frogs were injected with 625 IU of HCG to induce egg laying and housed individually in 100 mM NaCl. 20–22 h later, eggs from each frog were inspected and batches containing high quality (<5% aberrant morphology) eggs were pooled. Eggs were then stirred in L-cysteine buffer (2.2% cysteine-HCl, pH7.7) for 8 min, washed 3 times with 0.5X MMR buffer (50 mM NaCl, 1 mM KCl, 0.25 mM $MgSO_4$, 1.25 mM $CaCl_2$, 2.5 mM HEPES, 0.05 mM EDTA, pH 7.8), and washed 3 times with Egg Lysis Buffer (250 mM Sucrose, 2.5 mM $MgCl_2$, 50 mM KCl, 1 mM DTT, 50 μg/mL cycloheximide, 10 mM HEPES pH7.7). Eggs were then allowed to settle, and supernatant was discarded. Eggs were concentrated by centrifugation at 176 × g for 1 min and any remaining supernatant was discarded. Eggs were then supplemented with cytochalasin B (final concentration: 2.5 μg/mL), aprotinin (5 μg/mL), and leupeptin (5 μg/mL) before being lysed by centrifugation at 20,000 × g in a swinging bucket rotor at 4°C for 20 min. CIE was recovered with a needle and syringe then stored on ice.

To prepare High Speed Supernatant (HSS), 4–20 mL of CIE was supplemented with cycloheximide (final concentration: 50 μg/mL), DTT (final concentration: 1 mM), cytochalasin B (final concentration: 2.5 μg/mL), aprotinin (final concentration: 5 μg/mL), and leupeptin (final concentration: 5 μg/mL) then centrifuged at 260,000 × g in a swinging bucket rotor at 2°C for 33 min. Following centrifugation, lipids were aspirated and the soluble HSS was recovered, frozen in liquid nitrogen, then at stored at −80°C.

To prepare NucleoPlasmic Extract (NPE), 30–50 mL of CIE was supplemented with cycloheximide (final concentration: 50 μg/mL), DTT (final concentration: 1 mM), cytochalasin B (final concentration: 2.5 μg/mL), aprotinin (final concentration: 5 μg/mL), leupeptin (final concentration: 5 μg/mL), and nocodazole (final concentration: 3.3 μg/mL) then centrifuged at 20,000 × g in a swinging bucket rotor at 4°C for 10 min. Following centrifugation, lipids were aspirated and the remaining CIE was collected while leaving behind the membranous pellet that formed during centrifugation. CIE was then supplemented with creatine phosphokinase (final concentration: 5 μg/mL), phosphocreatine (final concentration: 20mM), and ATP (Final concentration: 2 mM) then incubated at room temperature for 5 min. Nuclear assembly was initiated by addition of demembranated sperm chromatin (final concentration: 4,400 sperm/μL) and proceeded for 60–90 min at room temperature with end-over-end rotation. Nuclear assembly reactions were then centrifuged at 20,000 × g in a swinging bucket rotor at 4°C for 2 min. The nucleoplasmic layer was recovered then centrifuged at 260,000 × g in a swinging bucket rotor at 4°C for 30 min.

Following centrifugation, lipids were aspirated and the soluble NPE was recovered, frozen in liquid nitrogen, then at stored at −80°C.

DNA replication in *Xenopus* egg extracts—Plasmid DNA (12.3 ng/μL final concentration) was incubated for 30 min with High Speed Supernatant (HSS) supplemented with nocodazole (3 ng/μL final concentration) and ATP regenerating system (ARS, final concentration: 20 mM phosphocreatine, 2 mM ATP and 5 ng/μL phosphokinase). Replication was initiated by addition of 2 volumes NucleoPlasmic Extract (NPE) supplemented with ARS, and DTT (2 mM final concentration). Reactions were stopped by addition of 10 volumes Stop solution (50 mM Tris-HCl pH 8, 25 mM EDTA, 0.5% SDS (w/v)) then treated with RNase (190 ng/ul final concentration) and Proteinase K (909 ng/ul). ICRF-193 (TOP2-i) was dissolved in DMSO and added at a final concentration of 200 μM (Figure 1) or 25 μM (Figure 3). Etoposide (ETO) was dissolved in DMSO and added at a final concentration of 28.3 μM.

To stall forks at a LacR array, 0.05 volumes of plasmid DNA harboring a *lacO* array (300 ng/μL) were incubated with 0.1 volumes LacR (18 μM) at room temperature for 90 min. Licensing mix was then prepared by adding 0.85 volumes of HSS supplemented with nocodazole (final concentration: 3 ng/μL) and ATP regenerating system (ARS, final concentration: 20 mM phosphocreatine, 2 mM ATP, 5 ng/μL creatine phosphokinase). Licensing and initiation of replication were performed as described above.

Analysis of replication intermediates—To analyze replication intermediates, replication reactions were supplemented with [α−^{32}P]dATP (final concentration: 67–240 nM) to radiolabel nascent DNA strands. In most cases, samples were directly analyzed by native agarose gel electrophoresis and autoradiography. To quantify DNA replication (%), whole lane signal was quantified using ImageJ and normalized to peak signal for each experimental condition. To analyze fork merger, DNA was purified by phenol:chloroform extraction and ethanol precipitation, then treated with XmnI (0.4 U/μL) for 1hour at 37°C prior to gel electrophoresis. In all cases gel electrophoresis was performed using a native agarose gel (1% (w/v)) at 5V/cm in TBE (1X).

2D gel electrophoresis—To monitor replication intermediates, purified DNA was digested with XmnI (as described above) and then separated on a 0.4% agarose gel at 1 V/cm. The gel was stained with 0.3 μg/mL ethidium bromide then lanes were excised and recast in a 1% gel containing 0.3 μg/mL ethidium bromide before being separated at 4.5V/cm. Radiolabeled DNA was detected by phosphorimaging.

To assess the extent of catenation, purified DNA was digested with 0.04 U/μL Nb.BbvCI and then separated on a 0.4% agarose gel at 0.9 V/cm. The gel was stained with 0.3 μg/mL ethidium bromide then lanes were excised and recast in a 1.2% gel containing 0.3 μg/mL ethidium bromide before being separated at 4.8V/cm. Radiolabeled DNA was detected by phosphorimaging. Catenation was quantified as the percentage total catenane signal within each catenated species. Catenation was plotted as cumulative frequency (‘running total’); for each catenated species, the percent signal was added to the signal from all lesser-catenated species.

Plasmid constructs—pJD156 (p[*lacO*x32]) was used for all experiments unless otherwise specified. pJD145 (CTRL, Figure 5), pJD152 (p[*lacO*x16]), pJD156 (p[*lacO*x32]) were previously described (Dewar et al. 2015).[38]

Protein purification—Biotinylated LacR was generated previously using bacteria.[55] Full length *Xenopus* MCM10 (xMCM10)[56] was purified from insect cells. To obtain purified xMCM10, Hi-5 cells were infected with baculovirus expressing xMCM10 for 48 h then lysed in 50 mM Tris buffer (pH 7.5), 500 mM NaCl, 10% (v/v) glycerol and homogenized by hand. xMCM10 was purified using Ni-NTA resin and pooled fractions were buffer exchanged into 50 mM Tris buffer (pH 7.5), 150 mM NaCl, 10% glycerol then further purified by ion exchange using a HiTrap Heparin HP column (Cytivia).

Antibodies—Antibodies targeting *Xenopus* TOP2α, RTEL1(Ab1), MCM6, MCM7, CDC45, PCNA, ORC2, and RPA were previously described.[15,33,50–54]

The MCM10 antibody was generated in this study against a purified polypeptide of *Xenopus* MCM10 composed of the following sequence:
SYSGHVPKKMARGANGLRERLCQGGFHYGGVSSMAYAATLGSTTAPKKTVQSTLS
NMVVRGAEAIALEARQKIAAAKNVVQTDEFKELMTLPTPGALNLKKHLSGVSPQA
NCGKEGQPIQSISASTLLKQQKQQMLNARKKRAEESQKRFLESTEKSEKSSTLTSSAC
SVFQSPKQGAEFPNAQKMATPKLGRGFAEGDDVLFFDISPPPAPKLSTSAEAKKLLAI
QKLQAKGQTLAKTDPNSIKRKRGSSS

The RTEL1(Ab2) antibody was generated in this study against a purified polypeptide of *Xenopus* RTEL1 composed of the following sequence:
TPTPKNDQKAGPVPLIGSDYQSPRPMAQSSTREALRKAKNLDSHVPSLKRKRDECSS
EMVPGSVCEAYKQEMPLSSHRPAGLLDALEHSEKRVQEDKAGEEKVSRLSTLSLQY
DKRLADEQRGGKRKIKIVQNQAPEETCPSDQKMTSASLFLASVKQSLSQENYSIFMA
AMADYKKNNDLQQLITHLRSLFCQDTAKYNLLRGFYQFIRPHHKHEFESACKDLTG
KGCGYKPEHSVPRAERE

Immunodepletion and rescue—To deplete TOP2α, RTEL1, and MCM10 from *Xenopus* egg extracts, 1.29 volumes Protein A-coupled magnetic beads (Dynabeads Protein A (30 μg/μL)) were bound to anti-Top2α or control IgGs (0.5 μg antibody per 1 μg beads). Antibody-bound beads were then incubated with 1 volume of NPE or 0.5 volumes HSS for 20 min at room temperature with end-over-end rotation and this was repeated once. Depleted extracts were then collected and used for DNA replication (as above). For co-depletion of two proteins, beads were combined for each round of depletion and the number of depletion rounds remained constant. In all experiments beads bound to control IgGs were used to ensure that the concentration beads and IgGs was identical for all conditions. For rescue experiments, xMcm10 was added to a final concentration of 100 ng/μL.

Analysis of chromatin-bound proteins—Plasmid Pull Downs and Western blotting were performed as described previously.[15] 1 volume of Streptavidin-coupled magnetic beads (Dynabeads M-280 Streptavidin, 10 mg/mL) was washed three times with 6 volumes of binding buffer (50 mM Tris-HCl pH 8, 150 mM NaCl, 1mM EDTA, 0.02% Tween 20 (V/

V)). Beads were then resuspended in 6 volumes of binding buffer supplemented with 1 pmol biotinylated LacR per 10 mg of beads and incubated for 40 min at room temperature with end-over-end rotation. Beads were washed twice with 9 volumes binding buffer, then twice with 9 volumes PPD buffer (20 mM HEPES pH7.7, 500 mM sucrose, 5 mM MgCl2, 100 mM KCl, 0.5 mg/mL BSA, 0.04% Tween (V/V)), before being resuspended in 5 volumes PPD buffer. 12 μL aliquots of resuspended beads were cooled on ice and allowed to settle. For each sample, 3 μL of reaction was withdrawn and added to 15 μL chilled beads, which were resuspended by pipetting up-and-down 40 times immediately after sample addition. Samples were stored on ice until the end of the experiment, then transferred to the cold room. Beads were resuspended by pipetting then incubated for 30 min with end-over-end rotation at 4°C. Beads were then pelleted, and the supernatant was removed. Beads were then washed twice with 400 μL Wash buffer (20 mM HEPES pH7.7, 5 mM MgCl2, 100 mM KCl, 0.25 mg/mL BSA, 0.03% Tween (V/V)) and proteins were eluted with Laemmli Sample buffer. Samples were analyzed by Western Blotting and quantified using ImageJ.

Chromatin mass spectrometry—Chromatin mass spectrometry ('CHROMASS')[28] was performed using modifications to analyze plasmid DNA.[26] Plasmid DNA was replicated in mock-treated extracts containing ICRF-193 (TOP2-i) or vehicle control (DMSO), as outlined above. In parallel plasmid DNA was replicated in TOP2α-depleted extracts containing vehicle control. At 18 min, plasmid DNA and associated proteins were captured on beads, as outlined above, then resuspended in 50 μL ELB (2.5 mM $MgCl_2$, 50 mM KCl, 250 mM sucrose, 10 mM HEPES-KOH pH 7.7) and transferred to a new tube. Supernatant was removed, and beads were resuspended in 50 μL freshly prepared denaturation buffer (8 M Urea, 100 mM Tris, pH 8.0). 1 μL DTT (1 M) was added to each tube and samples were incubated for 15–45 min at room temperature with end-over-end rotation. 6 μL chloroacetamide (0.55 M) was then added and samples were incubated a further 40 min at room temperature with end-over-end rotation in the dark. 1.5 μg LysC was then added and samples were incubated for 2 h at 30°C with end-over-end rotation. Supernatant was transferred to a fresh tube followed by the addition of 280 μL ammonium bicarbonate then 2.5 μg trypsin and samples were incubated overnight at 30°C. Trypsin digestion was halted by the addition of 20 μL trifluoroacetic acid (10% (V/V) in water) followed by addition of 105 μL NaCl (2 M). Samples were centrifuged for 10 min, 8,000 RCF, at room temperature. Each sample was then applied to activated STAGE tips (Nikkyo Technos) containing C18 resin. STAGE tips were then washed with formic acid (0.1% (V/V) in water) and stored at 4°C. Peptides were eluted from STAGE tips, as outlined below. The resultant material was then analyzed by liquid chromatography-tandem mass spectrometry and quantified using label-free quantification, as outlined below. For each condition 3 experimental replicates were analyzed.

Liquid chromatography-tandem mass spectrometry (LC-MS/MS) analysis—Peptides were eluted from STAGE tips with 70% acetonitrile, eluates were dried by speed vac centrifugation, and peptides were reconstituted in 6 μL of 0.1% formic acid for analysis by LC-coupled tandem mass spectrometry (LC-MS/MS). An analytical column was packed with 20cm of C18 reverse phase material (Jupiter, 3 μm beads, 300Å, Phenomenox). Peptides (2.5 μL) were loaded on the reverse phase analytical column (360 μm O.D. ×

100 μm I.D.) using a Dionex Ultimate 3000 nanoLC and autosampler. The mobile phase solvents consisted of 0.1% formic acid, 99.9% water (solvent A) and 0.1% formic acid, 99.9% acetonitrile (solvent B). Peptides were gradient-eluted at 350 nL/min using a 95-min gradient. The gradient was as follows: 1–78 min, 2–40% B; 78–85 min, 40–95% B; 85–86 min, 95% B; 86–87 min, 95–2% B; 87–95 min (column re-equilibration), 2% B. Peptides were analyzed using a data-dependent method on a Q Exactive Plus (Thermo Scientific) mass spectrometer, equipped with a nanoelectrospray ionization source. The instrument method consisted of MS1 using an AGC target value of 3e6, followed by up to 20 MS/MS scans of the most abundant ions detected in the preceding MS scan. The MS2 AGC target was set to 5e4, dynamic exclusion was set to 20s, HCD collision energy was set to 27 nce, and peptide match and isotope exclusion were enabled. MS/MS spectra were searched against a *Xenopus laevis* database with peptide matches being integrated from MS1 scans, collated to the protein level, and then normalized using MaxQuant-LFQ v1.5.2.8.[59]

Co-immunoprecipitation experiments—For the co-immunoprecipitation experiment in Figure S5B antibodies were bound to Protein A Sepharose beads overnight at 4 °C ata concentration of 1 μg antibody per 1 μL beads. Beads were then washed three times with phosphate buffered saline and twice with ELB (2.5 mM $MgCl_2$, 50 mM KCl, 250 mM sucrose, 10 mM HEPES-KOH pH 7.7) to remove unbound antibodies. After preparation of beads, NPE was thawed, diluted ten-fold in ELB, then treated with 2U/μL Benzonase for 10 min at room temperature to eliminate any residual DNA. NPE was then incubated with 0.2 volumes of antibody-bound beads and immunoprecipitation was performed for 2 h at 4°C. Supernatant was removed and beads were washed five times with ELB containing 0.1% (V/V) Triton X-100. Supernatants and beads were then resuspended in Laemmli sample buffer and analyzed by Western blotting. For all other co-immunoprecipitation experiments the immunodepletion protocol described above was used. After the final round of depletion, beads were washed with 50 μL ELB (2.5 mM $MgCl_2$, 50 mM KCl, 250 mM sucrose, 10 mM HEPES-KOH pH 7.7) then transferred to a new tube. Supernatants and beads were then resuspended in Laemmli sample buffer, bead elutes were combined, and all samples were analyzed by Western blotting.

DNA-protein crosslink (DPCs) detection assay—DNA replication reactions were stopped by addition of 10 volumes Stop solution then treated with RNase, as outlined above. 0.2 volumes of radiolabeled control plasmid (pJD145, 0.25 ng/μL) was added to each sample, which was then split in two. Half the reaction was then treated with Proteinase K (889 ng/μL) while the other half was treated with vehicle control (de-ionized water). DNA was then purified by phenol:chloroform extraction and ethanol precipitation. Purified DNA samples were then separated by gel electrophoresis and visualized by autoradiography to detect total DNA (Proteinase K treated samples) or non-crosslinked DNA (samples not treated with Proteinase K). For each sample, fraction of DNA molecules containing DPCs was calculated using the total lane signal for non-crosslinked DNA (ncDNA) and total DNA (totDNA) normalized to control plasmid (CTRL) as follows: [(totDNA/CTRL) − (ncDNA/CTRL)]/(totDNA/CTRL) × 100%.

Nick translation of DNA—To radiolabel parental DNA strands, 8 μL of plasmid DNA (100–150 ng/μL) was added to 1 μL of NEB Buffer 2.1 (10X) and incubated with 1 μL Nb.BssSI (10 units/μl) at 37°C for 1 h, followed by heat inactivation at 80°C for 20 min. The mix was then supplemented with 0.5 μL NEB Buffer 2.1 (10X), 2.5 μL dNTPs (25 mM each of dCTP, dGTP, dTTP), 1.5 μL *E. coli* DNA Polymerase 1 (10 U/μL), and 0.5 μL [α^{32}P]-dATP (3.33 μM), then incubated at 16°C for 10 min. For control unlabeled samples, a parallel reaction was performed where 0.5 μL of unlabeled dATP (3.33 μM) was added. Nick-translated DNA was then buffer exchanged into 10 mM Tris (pH 7.4) using micro Bio-Spin columns (Bio-Rad) and used for replication.

QUANTIFICATION AND STATISTICAL ANALYSIS

Statistical analysis of label free quantification—Resulting protein quantitative outputs were compared pairwise using ProStar (live.prostar-proteomics.org).[57] All calculations were based on the LFQ intensities reported by MaxQuant. To identify proteins that were significantly up-regulated in TOP2-i treated or TOP2α-depleted conditions compared with control reactions a modified t-test was performed using Prostar with Benjamini-Hochberg correction for multiple comparisons applied to correct for false positives. All test results are reported in Table S2.

Supplementary Material

Refer to Web version on PubMed Central for supplementary material.

ACKNOWLEDGMENTS

J.M.D. was supported by NIH grant R35GM128696. B.F.E. was supported by NIH grant R35GM136401. L.V.C. received support from T32-CA009582, and E.J.V. received support from T32-ES007028. Jesus Mallol Diaz provided experimental assistance.

REFERENCES

1. Bell SP, and Labib K (2016). Chromosome duplication in Saccharomyces cerevisiae. Genetics 203, 1027–1067. 10.1534/genetics.115.186452. [PubMed: 27384026]
2. Bleichert F, Botchan MR, and Berger JM (2017). Mechanisms for initiating cellular DNA replication. Science 355, aah6317. 10.1126/science.aah6317.
3. O'Donnell M, Langston L, and Stillman B (2013). Principles and concepts of DNA replication in bacteria, archaea, and eukarya. Cold Spring Harb. Perspect. Biol. 5, a010108. 10.1101/cshperspect.a010108. [PubMed: 23818497]
4. Siddiqui K, On KF, and Diffley JFX (2013). Regulating DNA replication in eukarya. Cold Spring Harb. Perspect. Biol. 5, a012930. 10.1101/cshperspect.a012930. [PubMed: 23838438]
5. Huberman JA, and Riggs AD (1968). On the mechanism of DNA replication in mammalian chromosomes. J. Mol. Biol. 32, 327–341. [PubMed: 5689363]
6. McIntosh D, and Blow JJ (2012). Dormant origins, the licensing checkpoint, and the response to replicative stresses. Cold Spring Harb. Perspect. Biol. 4, a012955. 10.1101/cshperspect.a012955. [PubMed: 22904560]
7. Limas JC, and Cook JG (2019). Preparation for DNA replication: the key to a successful S phase. FEBS Lett. 593, 2853–2867. 10.1002/1873-3468.13619. [PubMed: 31556113]
8. Cortez D (2019). Replication-coupled DNA repair. Mol. Cell 74, 866–876. 10.1016/j.molcel.2019.04.027. [PubMed: 31173722]

9. Seidman MM, and Salzman NP (1979). Late replicative intermediates are accumulated during simian virus 40 DNA replication in vivo and in vitro. J. Virol. 30, 600–609. [PubMed: 224218]
10. Tapper DP, and DePamphilis ML (1978). Discontinuous DNA replication: accumulation of Simian virus 40 DNA at specific stages in its replication. J. Mol. Biol. 120, 401–422. [PubMed: 206700]
11. Deegan TD, Baxter J, Ortiz Bazán MÁ, Yeeles JTP, and Labib KPM (2019). Pif1-Family helicases support fork convergence during DNA replication termination in eukaryotes. Mol. Cell 74, 231–244.e9. 10.1016/j.molcel.2019.01.040. [PubMed: 30850330]
12. Devbhandari S, Jiang J, Kumar C, Whitehouse I, and Remus D (2017). Chromatin constrains the initiation and elongation of DNA replication. Mol. Cell 65, 131–141. 10.1016/j.molcel.2016.10.035. [PubMed: 27989437]
13. Ishimi Y, Sugasawa K, Hanaoka F, Eki T, and Hurwitz J (1992). Topoisomerase II plays an essential role as a swivelase in the late stage of SV40 chromosome replication in vitro. J. Biol. Chem. 267, 462–466. [PubMed: 1309747]
14. Hiasa H, and Marians KJ (1996). Two distinct modes of strand unlinking during theta-type DNA replication. J. Biol. Chem. 271, 21529–21535. [PubMed: 8702938]
15. Heintzman DR, Campos LV, Byl JAW, Osheroff N, and Dewar JM (2019). Topoisomerase II is crucial for fork convergence during vertebrate replication termination. Cell Rep. 29, 422–436.e5. 10.1016/j.celrep.2019.08.097. [PubMed: 31597101]
16. Pommier Y, Sun Y, Huang SYN, and Nitiss JL (2016). Roles of eukaryotic topoisomerases in transcription, replication and genomic stability. Nat. Rev. Mol. Cell Biol. 17, 703–721. 10.1038/nrm.2016.111. [PubMed: 27649880]
17. Vos SM, Tretter EM, Schmidt BH, and Berger JM (2011). All tangled up: how cells direct, manage and exploit topoisomerase function. Nat. Rev. Mol. Cell Biol. 12, 827–841. 10.1038/nrm3228. [PubMed: 22108601]
18. Ullsperger CJ, Vologodskii AV, and Cozzarelli NR (1995). Unlinking of DNA by topoisomerases during DNA replication. In Nucleic Acids and Molecular Biology, Eckstein F and Lilley DMJ, eds. (Springer Berlin Heidelberg), pp. 115–142. 10.1007/978-3-642-79488-9_6.
19. Le TT, Gao X, Park SH, Lee J, Inman JT, Lee JH, Killian JL, Badman RP, Berger JM, and Wang MD (2019). Synergistic coordination of chromatin torsional mechanics and topoisomerase activity. Cell 179, 619–631.e15. 10.1016/j.cell.2019.09.034. [PubMed: 31626768]
20. Champoux JJ, and Been MD (1980). Mechanistic studies of DNA replication and genetic recombination. In ICN-UCLA Symposia on Molecular and Cellular Biology, Albert B, ed. (Academic Press).
21. Baxter J, and Diffley JFX (2008). Topoisomerase II inactivation prevents the completion of DNA replication in budding yeast. Mol. Cell 30, 790–802. 10.1016/j.molcel.2008.04.019. [PubMed: 18570880]
22. Ivessa AS, Zhou JQ, and Zakian VA (2000). The Saccharomyces Pif1p DNA helicase and the highly related Rrm3p have opposite effects on replication fork progression in ribosomal DNA. Cell 100, 479–489. [PubMed: 10693764]
23. Sabouri N, McDonald KR, Webb CJ, Cristea IM, and Zakian VA (2012). DNA replication through hard-to-replicate sites, including both highly transcribed RNA Pol II and Pol III genes, requires the S. pombe Pfh1 helicase. Genes Dev. 26, 581–593. 10.1101/gad.184697.111. [PubMed: 22426534]
24. Steinacher R, Osman F, Dalgaard JZ, Lorenz A, and Whitby MC (2012). The DNA helicase Pfh1 promotes fork merging at replication termination sites to ensure genome stability. Genes Dev. 26, 594–602. 10.1101/gad.184663.111. [PubMed: 22426535]
25. Suski C, and Marians KJ (2008). Resolution of converging replication forks by RecQ and topoisomerase III. Mol. Cell 30, 779–789. 10.1016/j.molcel.2008.04.020. [PubMed: 18570879]
26. Larsen NB, Gao AO, Sparks JL, Gallina I, Wu RA, Mann M, Räschle M, Walter JC, and Duxin JP (2019). Replication-coupled DNA-protein crosslink repair by SPRTN and the proteasome in Xenopus egg extracts. Mol. Cell 73, 574–588.e7. 10.1016/j.molcel.2018.11.024. [PubMed: 30595436]
27. Dewar JM, Low E, Mann M, Räschle M, and Walter JC (2017). CRL2(Lrr1) promotes unloading of the vertebrate replisome from chromatin during replication termination. Genes Dev. 31, 275–290. 10.1101/gad.291799.116. [PubMed: 28235849]

28. Räschle M, Smeenk G, Hansen RK, Temu T, Oka Y, Hein MY, Nagaraj N, Long DT, Walter JC, Hofmann K, et al. (2015). DNA repair. Proteomics reveals dynamic assembly of repair complexes during bypass of DNA cross-links. Science 348, 1253671. 10.1126/science.1253671. [PubMed: 25931565]
29. Roca J, Ishida R, Berger JM, Andoh T, and Wang JC (1994). Antitumor bisdioxopiperazines inhibit yeast DNA topoisomerase II by trapping the enzyme in the form of a closed protein clamp. Proc. Natl. Acad. Sci. USA 91, 1781–1785. 10.1073/pnas.91.5.1781. [PubMed: 8127881]
30. Parisis N, Krasinska L, Harker B, Urbach S, Rossignol M, Camasses A, Dewar J, Morin N, and Fisher D (2017). Initiation of DNA replication requires actin dynamics and formin activity. EMBO J. 36, 3212–3231. 10.15252/embj.201796585. [PubMed: 28982779]
31. Velkova A, Carvalho MA, Johnson JO, Tavtigian SV, and Monteiro ANA (2010). Identification of Filamin A as a BRCA1-interacting protein required for efficient DNA repair. Cell Cycle 9, 1421–1433. 10.4161/cc.9.7.11256. [PubMed: 20305393]
32. Zhou ZX, Lujan SA, Burkholder AB, Garbacz MA, and Kunkel TA (2019). Roles for DNA polymerase d in initiating and terminating leading strand DNA replication. Nat. Commun. 10, 3992. 10.1038/s41467-019-11995-z. [PubMed: 31488849]
33. Sparks JL, Chistol G, Gao AO, Räschle M, Larsen NB, Mann M, Duxin JP, and Walter JC (2019). The CMG helicase bypasses DNA-protein cross-links to facilitate their repair. Cell 176, 167–181.e21. 10.1016/j.cell.2018.10.053. [PubMed: 30595447]
34. Langston LD, Mayle R, Schauer GD, Yurieva O, Zhang D, Yao NY, Georgescu RE, and O'Donnell ME (2017). Mcm10 promotes rapid isomerization of CMG-DNA for replisome bypass of lagging strand DNA blocks. Elife 6, e29118. 10.7554/eLife.29118. [PubMed: 28869037]
35. Douglas ME, Ali FA, Costa A, and Diffley JFX (2018). The mechanism of eukaryotic CMG helicase activation. Nature 555, 265–268. 10.1038/nature25787. [PubMed: 29489749]
36. Chadha GS, Gambus A, Gillespie PJ, and Blow JJ (2016). Xenopus Mcm10 is a CDK-substrate required for replication fork stability. Cell Cycle 15, 2183–2195. 10.1080/15384101.2016.1199305. [PubMed: 27327991]
37. Wasserman MR, Schauer GD, O'Donnell ME, and Liu S (2019). Replication fork activation is enabled by a single-stranded DNA gate in CMG helicase. Cell 178, 600–611.e16. 10.1016/j.cell.2019.06.032. [PubMed: 31348887]
38. Dewar JM, Budzowska M, and Walter JC (2015). The mechanism of DNA replication termination in vertebrates. Nature 525, 345–350. 10.1038/nature14887. [PubMed: 26322582]
39. Wohlschlegel JA, Dhar SK, Prokhorova TA, Dutta A, and Walter JC (2002). Xenopus Mcm10 binds to origins of DNA replication after Mcm2–7 and stimulates origin binding of Cdc45. Mol. Cell 9, 233–240. 10.1016/s1097-2765(02)00456-2. [PubMed: 11864598]
40. Vannier JB, Sandhu S, Petalcorin MIR, Wu X, Nabi Z, Ding H, and Boulton SJ (2013). RTEL1 is a replisome-associated helicase that promotes telomere and genome-wide replication. Science 342, 239–242. 10.1126/science.1241779. [PubMed: 24115439]
41. Nitiss JL (2009). Targeting DNA topoisomerase II in cancer chemotherapy. Nat. Rev. Cancer 9, 338–350. 10.1038/nrc2607. [PubMed: 19377506]
42. Van Ravenstein SX, Mehta KP, Kavlashvili T, Byl JAW, Zhao R, Osheroff N, Cortez D, and Dewar JM (2022). Topoisomerase II poisons inhibit vertebrate DNA replication through distinct mechanisms. EMBO J. 41, e110632. 10.15252/embj.2022110632. [PubMed: 35578785]
43. Duxin JP, Dewar JM, Yardimci H, and Walter JC (2014). Repair of a DNA-protein crosslink by replication-coupled proteolysis. Cell 159, 346–357. 10.1016/j.cell.2014.09.024. [PubMed: 25303529]
44. Umbreit NT, Zhang CZ, Lynch LD, Blaine LJ, Cheng AM, Tourdot R, Sun L, Almubarak HF, Judge K, Mitchell TJ, et al. (2020). Mechanisms generating cancer genome complexity from a single cell division error. Science 368, eaba0712. 10.1126/science.aba0712. [PubMed: 32299917]
45. Fachinetti D, Bermejo R, Cocito A, Minardi S, Katou Y, Kanoh Y, Shirahige K, Azvolinsky A, Zakian VA, and Foiani M (2010). Replication termination at eukaryotic chromosomes is mediated by Top2 and occurs at genomic loci containing pausing elements. Mol. Cell 39, 595–605. 10.1016/j.molcel.2010.07.024. [PubMed: 20797631]

46. McGuffee SR, Smith DJ, and Whitehouse I (2013). Quantitative, genome-wide analysis of eukaryotic replication initiation and termination. Mol. Cell 50, 123–135. 10.1016/j.molcel.2013.03.004. [PubMed: 23562327]
47. Baxley RM, Leung W, Schmit MM, Matson JP, Yin L, Oram MK, Wang L, Taylor J, Hedberg J, Rogers CB, et al. (2021). Bi-allelic MCM10 variants associated with immune dysfunction and cardiomyopathy cause telomere shortening. Nat. Commun. 12, 1626. 10.1038/s41467-021-21878-x. [PubMed: 33712616]
48. Vannier JB, Pavicic-Kaltenbrunner V, Petalcorin MIR, Ding H, and Boulton SJ (2012). RTEL1 dismantles T loops and counteracts telomeric G4-DNA to maintain telomere integrity. Cell 149, 795–806. 10.1016/j.cell.2012.03.030. [PubMed: 22579284]
49. Claussin C, Vazquez J, and Whitehouse I (2022). Single-molecule mapping of replisome progression. Mol. Cell 82, 1372–1382.e4. 10.1016/j.molcel.2022.02.010. [PubMed: 35240057]
50. Semlow DR, Zhang J, Budzowska M, Drohat AC, and Walter JC (2016). Replication-dependent unhooking of DNA interstrand cross-links by the NEIL3 glycosylase. Cell 167, 498–511.e14. 10.1016/j.cell.2016.09.008. [PubMed: 27693351]
51. Fang F, and Newport JW (1993). Distinct roles of cdk2 and cdc2 in RP-A phosphorylation during the cell cycle. J. Cell Sci. 106, 983–994. 10.1242/jcs.106.3.983. [PubMed: 8308077]
52. Mimura S, and Takisawa H (1998). Xenopus Cdc45-dependent loading of DNA polymerase alpha onto chromatin under the control of S-phase Cdk. EMBO J. 17, 5699–5707. 10.1093/emboj/17.19.5699. [PubMed: 9755170]
53. Kochaniak AB, Habuchi S, Loparo JJ, Chang DJ, Cimprich KA, Walter JC, and van Oijen AM (2009). Proliferating cell nuclear antigen uses two distinct modes to move along DNA. J. Biol. Chem. 284, 17700–17710. 10.1074/jbc.M109.008706. [PubMed: 19411704]
54. Walter J, and Newport J (2000). Initiation of eukaryotic DNA replication: origin unwinding and sequential chromatin association of Cdc45, RPA, and DNA polymerase alpha. Mol. Cell 5, 617–627. [PubMed: 10882098]
55. Kavlashvili T, Liu W, Mohamed TM, Cortez D, and Dewar JM (2023). Replication fork uncoupling causes nascent strand degradation and fork reversal. Nat. Struct. Mol. Biol. 30, 115–124. 10.1038/s41594-022-00871-y. [PubMed: 36593312]
56. Du W, Josephrajan A, Adhikary S, Bowles T, Bielinsky AK, and Eichman BF (2013). Mcm10 self-association is mediated by an N-terminal coiled-coil domain. PLoS One 8, e70518. 10.1371/journal.pone.0070518. [PubMed: 23894664]
57. Wieczorek S, Combes F, Lazar C, Giai Gianetto Q, Gatto L, Dorffer A, Hesse AM, Couté Y, Ferro M, Bruley C, and Burger T (2017). DAPAR & ProStaR: software to perform statistical analyses in quantitative discovery proteomics. Bioinformatics 33, 135–136. 10.1093/bioinformatics/btw580. [PubMed: 27605098]
58. Lebofsky R, Takahashi T, and Walter JC (2009). DNA replication in nucleus-free Xenopus egg extracts. Methods Mol. Biol. 521, 229–252. 10.1007/978-1-60327-815-7_13.
59. Cox J, Hein MY, Luber CA, Paron I, Nagaraj N, and Mann M (2014). Accurate proteome-wide label-free quantification by delayed normalization and maximal peptide ratio extraction, termed MaxLFQ. Mol. Cell. Proteomics 13, 2513–2526. 10.1074/mcp.M113.031591. [PubMed: 24942700]

Highlights

- Proteomic analysis of terminating replication forks identifies RTEL1 and MCM10
- Fork stalling during termination is overcome by RTEL1 and MCM10
- RTEL1 and MCM10 physically interact and functionally cooperate during termination
- Fork stalling prior to termination is also overcome by RTEL1 and MCM10

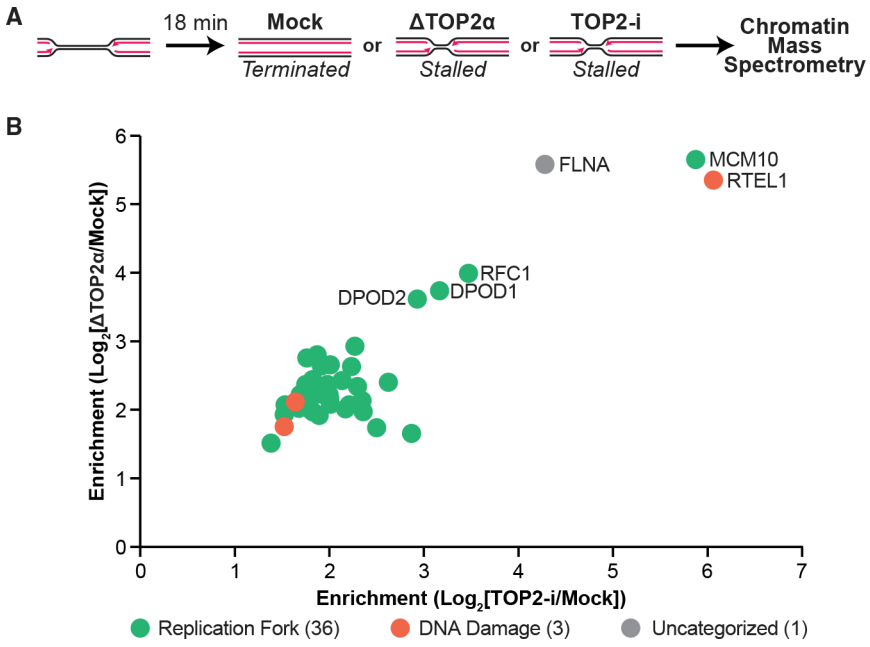

Figure 1. Proteomic analysis of replication forks stalled by topological stress

(A) Plasmid DNA was replicated in *Xenopus* egg extracts that were either mock-immunodepleted (Mock), TOP2α-immunodepleted (ΔTOP2α), or treated with TOP2 inhibitor ICRF-193 (TOP2-i). At 18 min, reactions were stopped, and DNA-bound proteins were analyzed by chromatin mass spectrometry and label-free quantification.

(B) Proteins from (A) that were ≥2-fold enriched in ΔTOP2α and TOP2-i conditions compared with mock are plotted according to their enrichment. Each protein was manually assigned a category. The six most highly enriched proteins are labeled. Values were calculated from three biological replicates for each condition. See also Figure S1C and Tables S1 and S2.

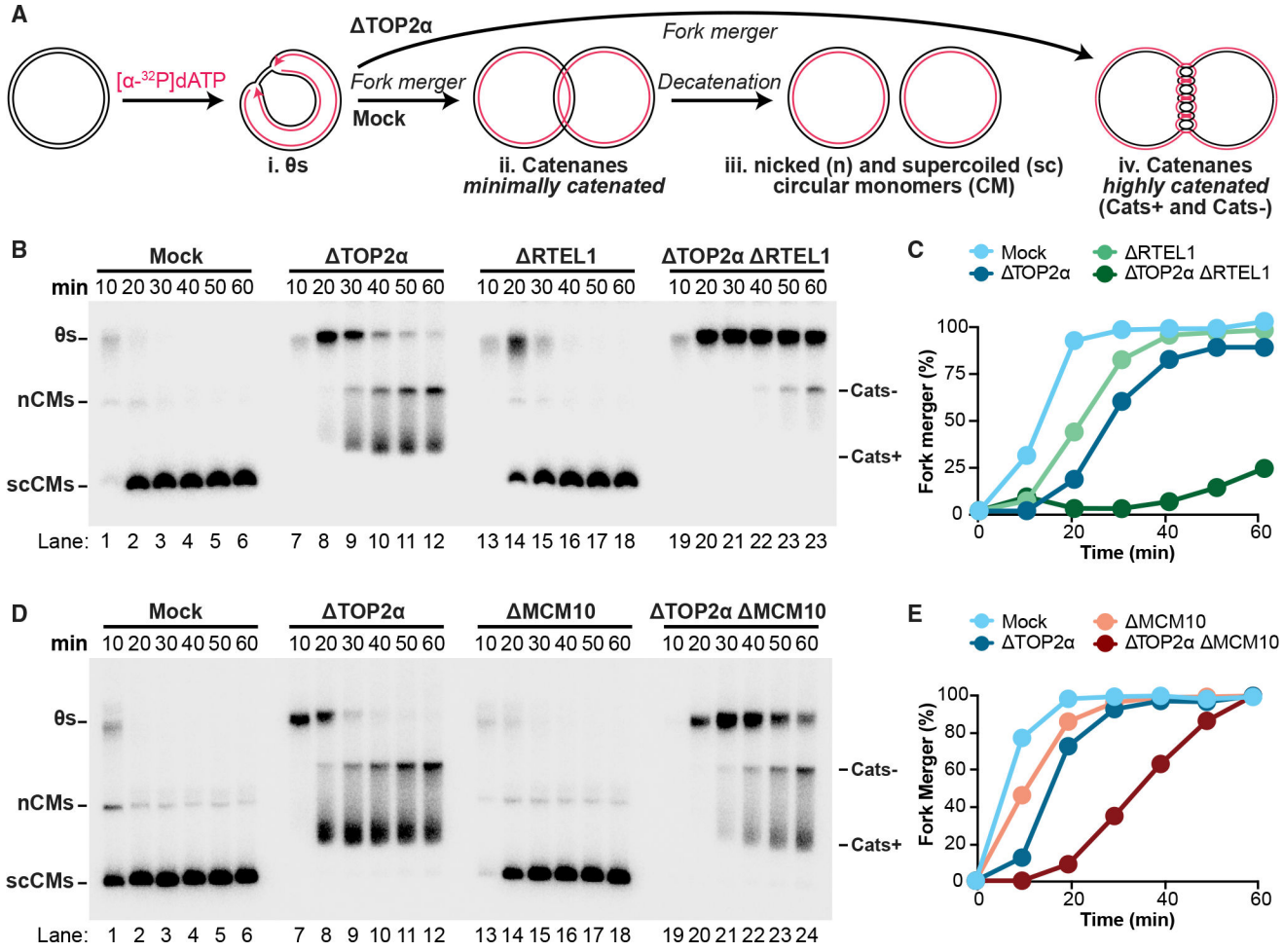

Figure 2. RTEL1 and MCM10 promote fork merger in the absence of TOP2α

(A) Plasmid DNA was replicated using *Xenopus* egg extracts in the presence of [α−^{32}P]dATP to label newly synthesized DNA strands under mock-depleted and ΔTOP2α-depleted conditions. The expected DNA structures, identified in Dewar et al.[38] and Heintzman et al.,[15] are indicated.

(B) Replication was performed as in (A) with and without co-depletion of RTEL1. Samples were separated on a native agarose gel and visualized by autoradiography.

(C) Quantification of fork merger from (B). See also Figure S2A. A biological replicate is shown in Figure S2B.

(D) Replication was performed as in (A) with and without co-depletion of MCM10. Samples were separated on a native agarose gel and visualized by autoradiography.

(E) Quantification of fork merger from (D). See also Figure S3A. A biological replicate is shown in Figure S3B.

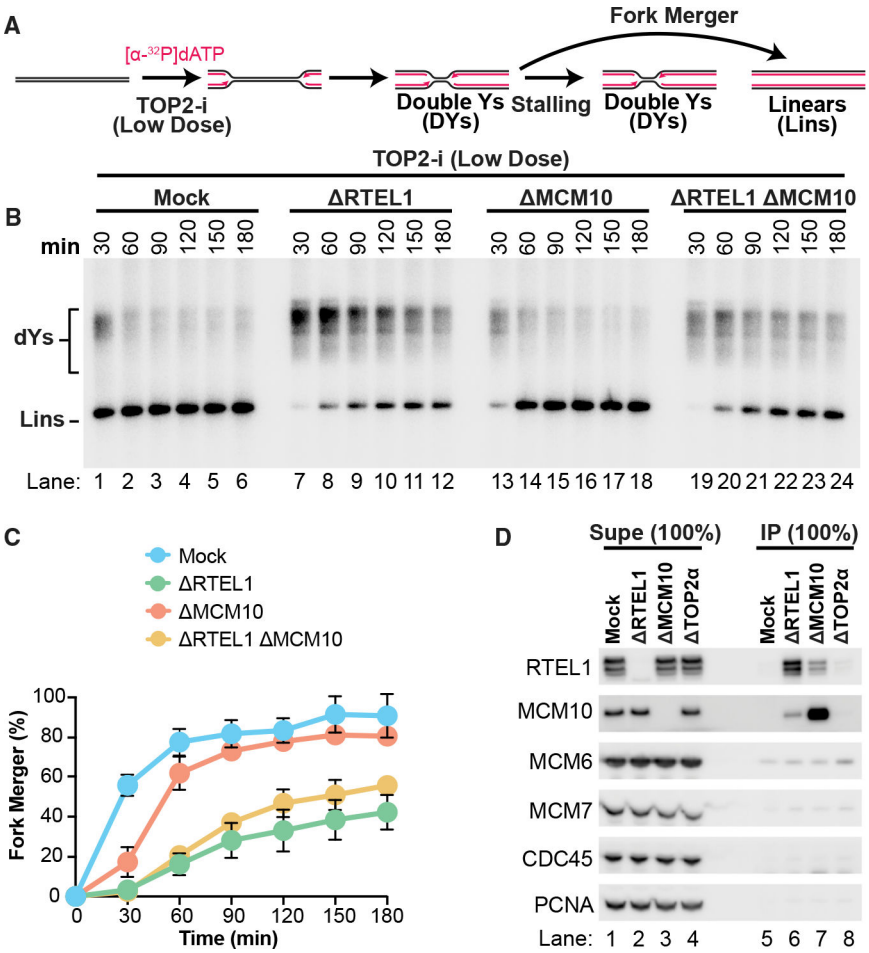

Figure 3. RTEL1 and MCM10 cooperate to promote fork merger

(A) Plasmid DNA was replicated in the presence of a low concentration of TOP2-i using extracts that were mock-depleted (mock) or depleted of RTEL1 (ΔRTEL1), MCM10 (ΔMCM10), or both (ΔRTEL1 ΔMCM10). Plasmids were purified and digested with XmnI, which cuts the plasmid once and allows unambiguous identification of replication fork structures ("DYs") and fully replicated molecules ("Lins") so that fork merger can be measured.

(B) Replication was performed as in (A). Samples were separated on a native agarose gel and visualized by autoradiography. See also Figure S4A.

(C) Quantification of fork merger from (B). Mean ± SD, n = 3 biological replicates. See also Figures S4B–S4D.

(D) DNA-free *Xenopus* egg extracts were mock-treated (mock) or immunoprecipitated with antibodies targeting RTEL1 (ΔRTEL1), MCM10 (ΔMCM10), or TOP2α (ΔTOP2α). The supernatant (Supe) and immunoprecipitate (IP) were then analyzed by western blotting. The multiple RTEL1 bands correspond to multiple isoforms in *Xenopus* egg extracts, as previously reported.[33] Increased MCM10 signal in the IP condition (lane 7) compared with Supe (lanes 1, 3, 4) may reflect competition between MCM10 and other proteins for binding to the membrane, compared with the comparatively pure IP sample. A representative experiment of two biological replicates is shown.

See also Figures S5A and S5B.

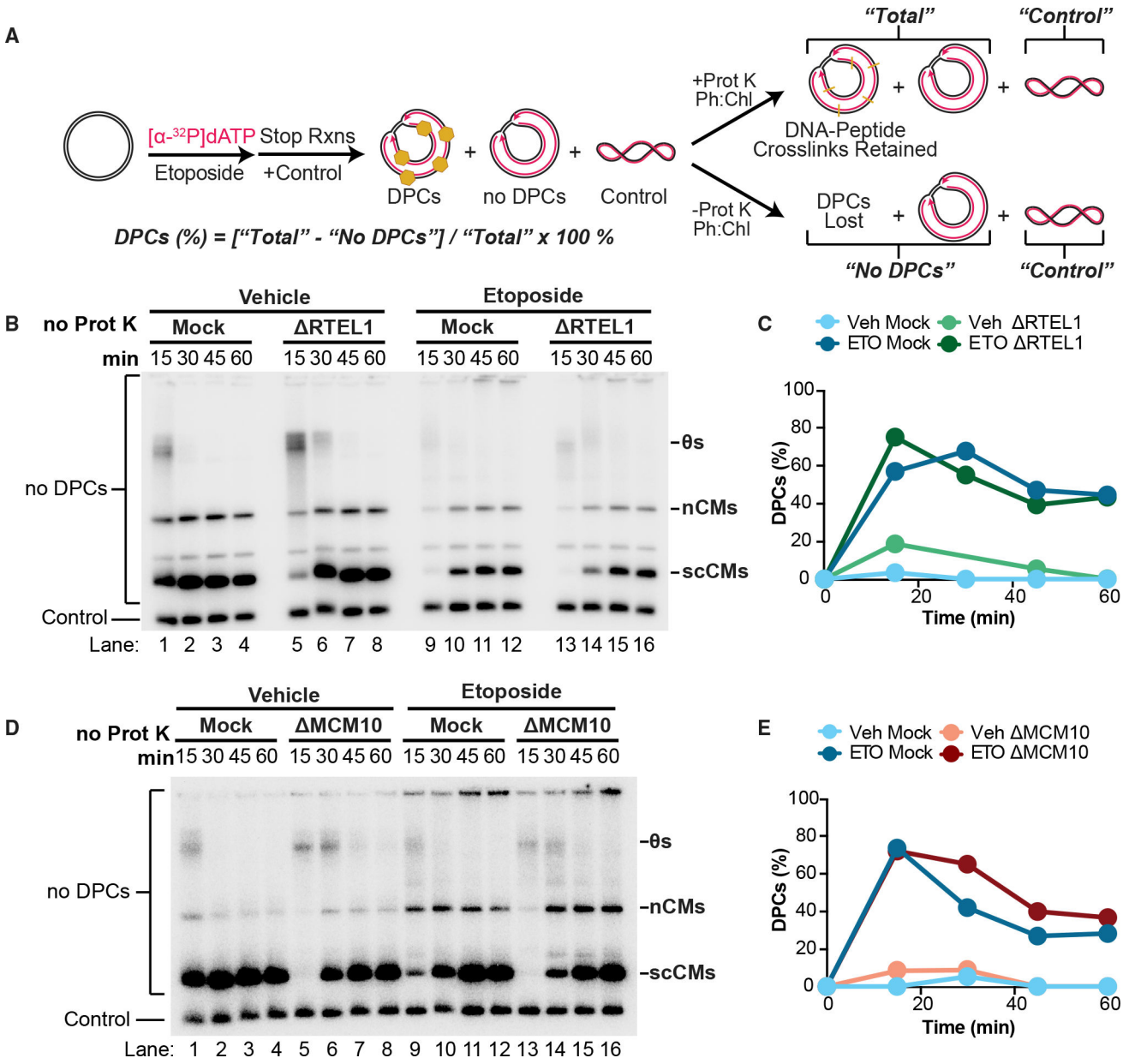

Figure 4. RTEL1 and MCM10 do not impact TOP2 utilization

(A) Plasmid DNA was replicated in the presence or absence of etoposide (ETO). Samples were combined with a radiolabeled control plasmid, then split and treated with or without proteinase K (Prot K), and purified by phenol:chloroform extraction. Without Prot K treatment, only replication intermediates lacking DPCs ("No DPCs") were recovered. With Prot K treatment, total replication intermediates were recovered ("Total"). Signal from replication intermediates was normalized to the loading control and then used to calculate the percentage of molecules containing DPCs at each time point, as indicated.

(B) Replication was performed as in (A) in mock-depleted (Mock) and RTEL1-depleted (ΔRTEL1) extracts. Samples that did not receive ProtK treatment were separated on a native

agarose gel and visualized by autoradiography. ProtK-treated samples are shown in Figure S6A.

(C) Quantification of DPC-containing molecules from (B) and Figure S6A. See also Figure S6B. An independent biological replicate is shown in Figure S6C.

(D) Replication was performed as in (A) in mock-depleted (Mock) and MCM10-depleted (ΔMCM10) extracts. Samples that did not receive ProtK treatment were separated on a native agarose gel and visualized by autoradiography. ProtK-treated samples are shown in Figure S6H.

(E) Quantification of DPC-containing molecules from (D) and Figure S6H. See also Figure S6I. An independent biological replicate is shown in Figure S6J.

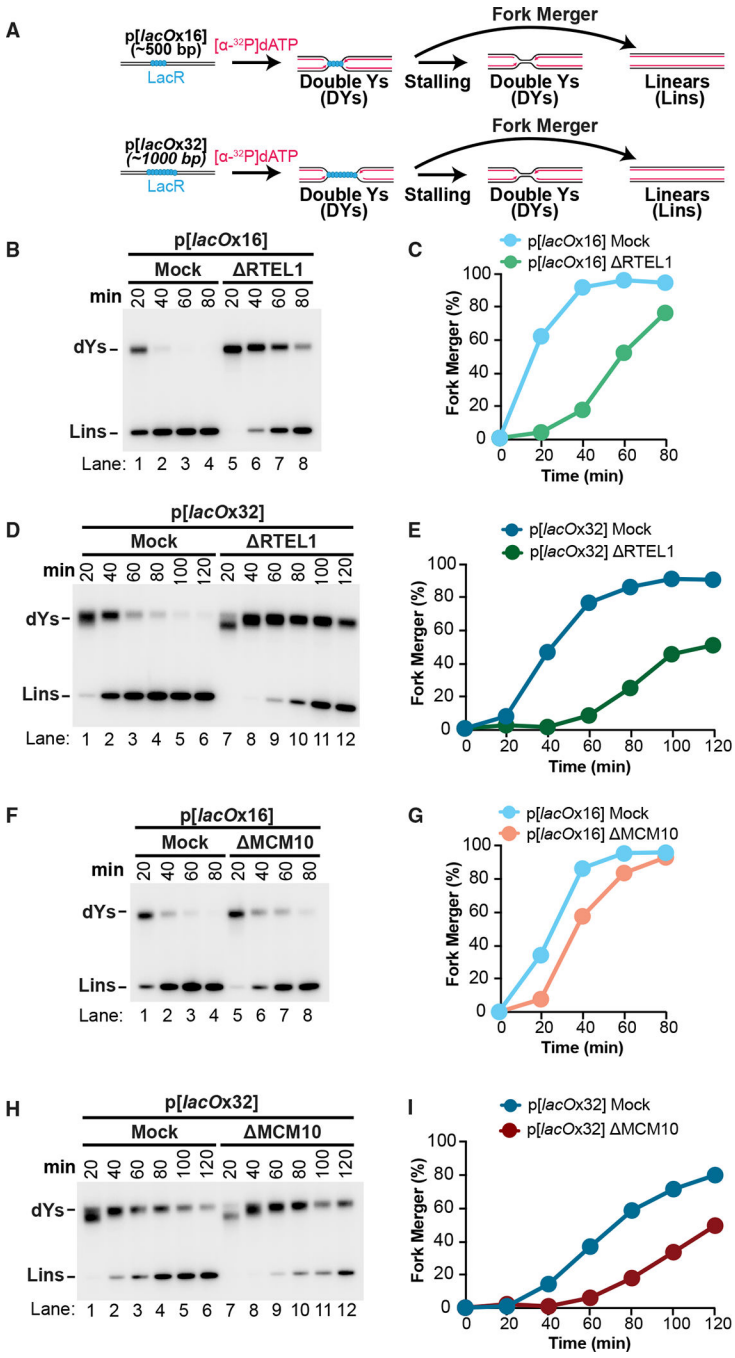

Figure 5. RTEL1 and MCM10 promote fork progression through a replication barrier

(A) Plasmid DNA harboring a 16x*lacO* array (p[*lacO*x16]) or a 32x*lacO* (p[*lacO*x32]) array was incubated with LacR to form an ~250 bp or ~500 bp replication barrier, respectively, then replicated. Purified replication intermediates were digested with XmnI, which cuts the plasmid once and allows unambiguous identification of replication fork structures ("DYs") and fully replicated molecules ("Lins") so that fork merger can be measured.

(B) p[*lacO*x16] was replicated as indicated in (A) using mock-depleted (Mock) and RTEL1-depleted (ΔRTEL1) extracts. Samples were separated on a native agarose gel and visualized by autoradiography.

(C) Quantification of fork merger from (B). An independent biological replicate is shown in Figure S7B.

(D) As part of the experiment depicted in (B), p[*lacO*x32] was replicated using mock-depleted (Mock) and RTEL1-depleted (ΔRTEL1) extracts.

(E) Quantification of fork merger from (D). An independent biological replicate is shown in Figure S7C.

(F) p[*lacO*x16] was replicated as indicated in (A) using mock-depleted (Mock) and MCM10-depleted (ΔMCM10) extracts. Samples were separated on a native agarose gel and visualized by autoradiography.

(G) Quantification of fork merger from (F). An independent biological replicate is shown in Figure S7E.

(H) As part of the experiment depicted in (F), p[*lacO*x32] was replicated using mock-depleted (Mock) and MCM10-depleted (ΔMCM10) extracts.

(I) Quantification of fork merger from (H). An independent biological replicate is shown in Figure S7F.

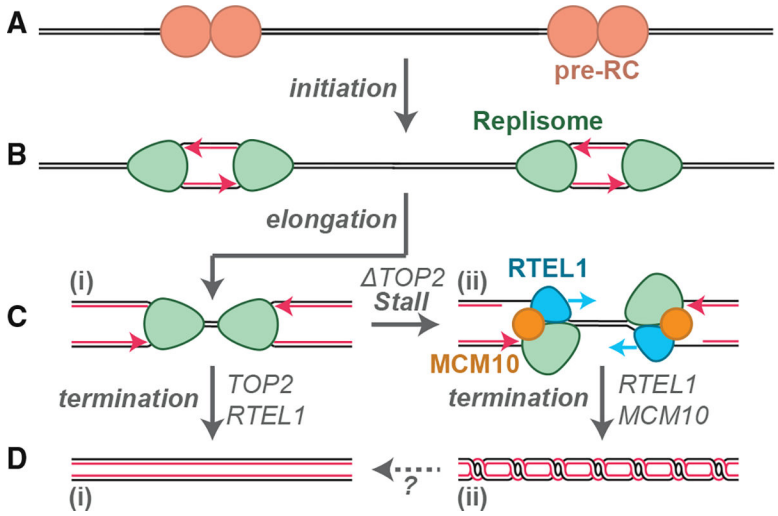

Figure 6. Model for vertebrate DNA replication

(A) Pre-RCs are loaded onto DNA prior to S phase.

(B) During S phase, pre-RCs are activated and associate with additional proteins to form replisomes that unwind DNA as they move away from each other in opposite directions ("initiation"). Activated replisomes then establish replication forks that duplicate DNA until they encounter an opposing fork ("elongation").

(C) (i) When two replication forks converge upon the same stretch of DNA ("termination"), they complete DNA synthesis without stalling or slowing, provided that TOP2 activity prevents accumulation of topological stress. RTEL1 also contributes to fork merger under unperturbed conditions, but its role is less clear (see discussion). (ii) In the absence of TOP2 activity, converging replication forks stall due to accumulation of topological stress. RTEL1 and MCM10 facilitate fork merger independently of TOP2.

(D) (i) The final products of replication termination are normally fully replicated and unlinked. (ii) If forks stall due to lack of TOP2 activity (Figure 6Cii), these products contain DNA catenanes. The fate of these structures and whether catenanes can be removed independently of TOP2 is unclear.

KEY RESOURCES TABLE

REAGENT or RESOURCE	SOURCE	IDENTIFIER
Antibodies		
Rabbit polyclonal anti-TOP2α	Heintzman et al.[15]	NEP4061
Rabbit polyclonal anti-RTELI(Abl)	Sparks et al.[33]	N/A
Rabbit polyclonal anti-RTEL1(Ab2)	This Study	NEP5204
Rabbit polyclonal anti-MCM10	This Study	NEP4723
Rabbit polyclonal anti-MCM6	Semlow et al.[50]	NEP2926
Rabbit polyclonal anti-MCM7	Fang et al.[51]	N/A
Rabbit polyclonal anti-CDC45	Mimura et al.[52]	N/A
Rabbit polyclonal anti-PCNA	Kochaniak et al.[53]	N/A
Rabbit polyclonal anti-ORC2	Fang et al.[51]	N/A
Rabbit polyclonal anti-RPA	Walter et al.[54]	N/A
Bacterial and virus strains		
E. coli NEB 5-alpha	New England Biolabs	C2987
Chemicals, peptides, and recombinant proteins		
LacR-biotin	Kavlashivili et al.[55]	N/A
Xenopus MCM10	Du et al.[56]	N/A
ICRF-193	Sigma	I4659
CDC7-i (PHA-767491)	Sigma	PZ0178
Proteinase K, recombinant	Roche	RPROTK-RO
RNase A, recombinant	Sigma	R4642
Glycogen	Roche	10901393001
[α-^{32}P]dATP	Perkin Elmer	BLU512Z250UC
Dynabeads Protein A	Invitrogen	10001D
Dynabeads M280 Streptavidin	Invitrogen	11205D
XmnI	New England Biolabs	R0194
Nb.BssSI	New England Biolabs	R0681
T4 Polynucleotide Kinase	New England Biolabs	M0201
ATP	Sigma	A7699
BSA	Sigma	A7906
Phosphocreatine	Sigma	P7936
DTT	Bio-Rad	1610611
Creatine PhosphoKinase (CPK)	Sigma	C3755
HCG	Sigma	CG10
LysC	Life Technologies	90307
Trypsin	Life Technologies	90305
Chloroacetamide	MP Biomedical	79-07-2
Ammonium Bicarbonate	Acros Organics	1066-33-7

REAGENT or RESOURCE	SOURCE	IDENTIFIER
Deposited data		
Raw proteomic data and MaxQuant output tables	ProteomeXchange	PXD031170
Experimental models: Organisms/strains		
Xenopus laevis (females)	Nasco	LM0053MX
Xenopus laevis (males)	Nasco	LM00715MX
Recombinant DNA		
p[lacOx16]	Dewar et al.[38]	pJD152
p[lacOx32]	Dewar et al.[38]	pJD156
CTRL	Dewar et al.[38]	pJD145
Software and algorithms		
ImageJ	National Institutes of Health	1.53k imagej.nih.gov/ij/download.html
Prostar	Wieczorek et al.[57]	live.prostar-proteomics.org